

# Inverse Multipath Fingerprinting for Millimeter Wave V2I Beam Alignment

Vutha Va, Junil Choi, Takayuki Shimizu, Gaurav Bansal, and Robert W. Heath, Jr.

**Abstract**—Efficient beam alignment is a crucial component in millimeter wave systems with analog beamforming, especially in fast-changing vehicular settings. This paper proposes a position-aided approach where the vehicle’s position (e.g., available via GPS) is used to query the multipath fingerprint database, which provides prior knowledge of potential pointing directions for reliable beam alignment. The approach is the inverse of fingerprinting localization, where the measured multipath signature is compared to the fingerprint database to retrieve the most likely position. The power loss probability is introduced as a metric to quantify misalignment accuracy and is used for optimizing candidate beam selection. Two candidate beam selection methods are derived, where one is a heuristic while the other minimizes the misalignment probability. The proposed beam alignment is evaluated using realistic channels generated from a commercial ray-tracing simulator. Using the generated channels, an extensive investigation is provided, which includes the required measurement sample size to build an effective fingerprint, the impact of measurement noise, the sensitivity to changes in traffic density, and a beam alignment overhead comparison with IEEE 802.11ad as the baseline. Using the concept of beam coherence time, which is the duration between two consecutive beam alignments, and parameters of IEEE 802.11ad, the overhead is compared in the mobility context. The results show that while the proposed approach provides increasing rates with larger antenna arrays, IEEE 802.11ad has decreasing rates due to the larger beam training overhead that eats up a large portion of the beam coherence time, which becomes shorter with increasing mobility.

**Index Terms**—Millimeter wave, vehicular communication, 5G mobile communication, beam alignment, position-aided.

## I. INTRODUCTION

Communication enhances advanced driver assistance systems, enables a wide range of infotainment options, and paves the way towards fully automated driving. Vehicular automation capabilities rely heavily on perception sensors such as camera, radar, and LIDAR [1]. Sharing the data from these sensors between vehicles, or with the infrastructure, can extend the sensing range as well as provide redundancy in case of sensor

failures. High data rate links with the infrastructure also enable map updates, edge-network control of vehicles, and a wider range of infotainment services. Unfortunately, the data rate requirements are increasing beyond what can be provided by the fourth generation (4G) cellular or Dedicated Short-Range Communication (DSRC) solutions [2]–[4].

Millimeter wave (mmWave) is a means to provide high data rates in vehicle-to-everything (V2X) settings [4], [5], thanks to the large spectral channels [5]. The need for adaptive antennas to overcome the shrinking antenna aperture at high frequencies is one of the main challenges in using mmWave [4], [5]. Due to the use of sharp beams and the high susceptibility to blockage, beam pointing directions have to be aligned and readjusted according to the changes in the environment. The high mobility in the vehicular context will require frequent beam realignment. Therefore, fast and efficient beam alignment is crucial in enabling high data rate mmWave vehicular communications.

Prior knowledge of the propagation environment can be used to reduce the beam alignment overhead. This paper focuses on the use of multipath fingerprints, which are the long-term multipath channel characteristics associated with locations. The term “fingerprint” originates from the localization literature [6]–[8], where the main premise is that channel characteristics are highly correlated with locations. In fingerprinting-based localization methods, there is a fingerprint database, which records fingerprints at different locations in the area of interest. When a terminal wants to localize itself, it first performs radio frequency (RF) channel measurements to obtain the multipath fingerprint at the current location. The obtained fingerprint is then matched against the fingerprints in the database and the output location is computed based on the match fingerprints in the database that are “closest” to the observed fingerprint. Considering the availability of position information in the vehicular context, we propose to use this idea in inverse. Localization is an important task in driving automation, where vehicles position themselves via a suite of sensors including Global Positioning System (GPS), cameras, and LIDAR [9]. This position information can be used to query the fingerprint database which is indexed by location to determine beam directions that are likely to provide satisfactory link quality. Because of the sparsity of mmWave channels [10], potential directions are expected to be highly concentrated and thus we expect a large reduction in the beam training overhead.

The objective of this paper is to develop an efficient beam alignment method suitable for a vehicle-to-infrastructure (V2I) setting. Our contributions are summarized as follows.

Vutha Va and Robert W. Heath, Jr. are with the Wireless Networking and Communications Group, The University of Texas at Austin, TX 78712-1687 USA (e-mail: vutha.va@utexas.edu, rheath@utexas.edu).

Junil Choi is with the Department of Electrical Engineering, Pohang University of Science and Technology (POSTECH), Pohang, Gyeongbuk, Korea 37673 (e-mail: junil@postech.ac.kr).

Takayuki Shimizu and Gaurav Bansal are with TOYOTA InfoTechnology Center, U.S.A., Inc., Mountain View, CA 94043 USA (e-mail: tshimizu@us.toyota-itc.com, gbansal@us.toyota-itc.com).

This work is supported in part by the U.S. Department of Transportation through the Data-Supported Transportation Operations and Planning (D-STOP) Tier 1 University Transportation Center and by the Texas Department of Transportation under Project 0-6877 entitled “Communications and Radar-Supported Transportation Operations and Planning (CAR-STOP)” and by a grant from TOYOTA InfoTechnology Center, U.S.A., Inc.

- We propose a novel and efficient beam alignment method using multipath fingerprints. In this paper, we consider an offline learning approach where there is a dedicated period of time for building the database before it is used for efficient beam alignment.
- Three types of fingerprints (Type A, B, and C) are proposed, which differ in how measurements are collected and stored. Type A assumes each contributing vehicle performs an exhaustive search over all beam pairs (so that correlation between beam pairs can be captured), while Type B and Type C collect only a few measurements at a time. Type A and Type B store the raw received power, while Type C fits the measurements to a distribution and only records the parameters of the distribution. This provides flexibility for actual implementations, where data collection and storage cost must be met.
- We introduce the power loss probability as a metric for evaluating the accuracy of the beam alignment. This metric leads to a mathematical framework to optimize the candidate beam pair selection. We propose two low complexity solutions, where one is a heuristic and the other is a solution that minimizes the misalignment probability.
- We provide an extensive numerical investigation, which includes the training sample size to build the fingerprint database, beam training overhead comparison with IEEE 802.11ad, and the sensitivity to changes in vehicular traffic density. For the overhead comparison, we leverage the concept of beam coherence time [11] to quantify the beam training cost in the vehicular context. We use realistic channels generated from a commercial ray-tracing simulator, Wireless InSite [12], in all our results.

We note that while we emphasize the V2I context in this work, the approach can also be applied to general cellular settings. An additional challenge is in how to determine the orientation of the antenna array of the user equipment (which is needed to translate angles of arrival and departure (AoAs/AoDs) to beam indices). This is not as important for vehicles because the array is fixed on the vehicle (e.g., the roof) and the orientation can be determined from the heading of the vehicle.

Beam alignment is a subject of intense research because of its importance in enabling mmWave communications. Here, we summarize and compare with relevant work in the context of analog beamforming, where both the transmitter and receiver have only one RF chain. We group existing solutions into four categories: beam sweeping [13]–[15], AoAs/AoDs estimation [16]–[18], blackbox optimization [19]–[21], and side information [22]–[26].

Beam sweeping involves a set of beam measurements designed to cover all possible pointing directions, whose simplest form is the exhaustive search. It is simple and robust because it makes few assumptions on the channel. It only requires that the spatial channel does not change during the sweeping time. This approach has been adopted in existing mmWave standards such as IEEE 802.15.3c [27] and IEEE 802.11ad [28] for indoor use cases. The brute force search measures all transmit and receive beam pair combinations resulting in quadratic complexity in the beam codebook size. Our approach

reduces the search time by prioritizing the most promising directions identified from the fingerprints. The beam search can also be done hierarchically [13]–[15], but the search time does not change much because large spreading is needed to use wide beams in the initial stage.

AoA/AoD estimation leverages the sparsity of mmWave channels to reduce the number of measurements required compared to beam sweeping. For example, compressive sensing is used in [16], [17] while an approximate maximum likelihood estimator is derived using the channel structure directly in [18]. Compressive measurements have to overcome the lack of antenna gain during the measurement phase, unlike our approach that uses narrow beams for the beam training.

Blackbox optimization is another approach to efficiently explore the beam directions [19]–[21]. This framework is based on the premise that there is some structure (e.g., smoothness) of the objective function (i.e., the received power here) and thus one does not have to blindly search all the beam pair combinations. This approach uses narrow beams in the initial search like our method, but it requires a larger number of feedbacks to navigate the search region and this feedback overhead will be the bottleneck in reducing the search time.

The final category uses side information available from sensors (including communication systems at other frequencies). The work in [22], [23] uses position information to determine beam directions. This can eliminate the beam training overhead but it only works in LOS channels. Radar information is used in [24], while information from lower frequencies is used in [25], [26]. Our proposed approach is in this category, where we use position information and multipath fingerprints. Unlike [22], [23], by leveraging multipath fingerprints, our approach can work in both LOS and non-LOS channels.

The rest of the paper is as follows. The system model is described in Section II. In Section III we define the multipath fingerprints and explain how the proposed beam alignment works. We provide an analytical framework to predict the alignment performance from the fingerprints in Section IV. In Section V, we present our beam candidate selection methods using the fingerprints. An extensive numerical investigation is provided in Section VI. Finally, the paper is concluded in Section VII.

## II. SYSTEM MODEL

This paper considers V2I communications in an urban street canyon environment with high traffic density, where LOS is often unavailable and represents a challenging scenario for beam alignment. While the methodology of the beam training is general, we test the approach using data from a commercial ray-tracing simulator, Wireless InSite [12]. The evaluations of the proposed method are conducted via post-processing in Matlab.

### A. Channel Model

The simulation environment is shown in Fig. 1. The considered urban street environment has two lanes. All the buildings are made of concrete, and the road surfaces are made of asphalt. We simulate two types of vehicles represented by

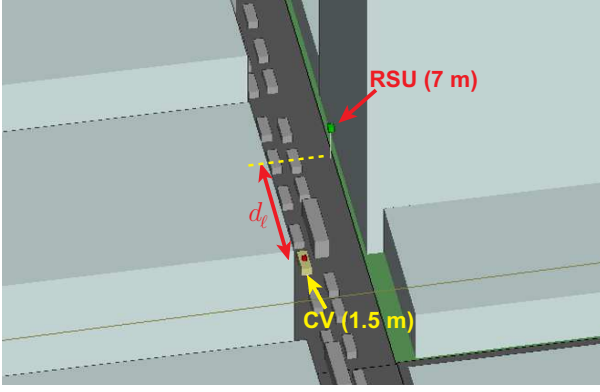


Fig. 1. Ray-tracing simulation environment. The numbers in the parenthesis are the antenna heights.

metal boxes: cars ( $1.8 \text{ m} \times 5 \text{ m} \times 1.5 \text{ m}$ ) and trucks ( $2.5 \text{ m} \times 12 \text{ m} \times 3.8 \text{ m}$ ). The ratio between cars and truck is set to 3:2. The roadside unit (RSU) is placed on the right side, and a car on the left lane is selected as the communicating vehicle (CV). The RSU antenna is 7 m above the ground and the antenna on the CV is placed on its roof at 1.5 m height. Because trucks are taller, they could block the LOS path between the CV and the RSU. The carrier frequency is set to 60 GHz.

To imitate the dynamics of the environment, we simulate multiple snapshots of the scenario where vehicles are independently and randomly placed in each snapshot. The gap between vehicles (i.e., from the front bumper to the rear bumper of the heading vehicle)  $\zeta$  is randomly determined from the Erlang distribution [29] given by

$$f_{\zeta}(\zeta) = \frac{(\kappa\mu_{\zeta})^{\kappa}}{(\kappa-1)!} \zeta^{\kappa-1} e^{-\kappa\mu_{\zeta}\zeta}, \quad (1)$$

where  $\kappa$  is the shape parameter and  $1/\mu_{\zeta}$  is the mean gap. Following [30],  $\kappa = 6$  and  $\mu_{\zeta} = 0.209$  are used in our simulation, which produces an average gap of 4.78 m. Since multipath fingerprints are associated with locations, we need to generate multiple channels at a given location. To do this, the CV is placed at a longitudinal distance  $d_{\ell}$  from the RSU (see Fig. 1), where  $d_{\ell}$  is uniformly drawn from  $[d_0 - \sigma_d, d_0 + \sigma_d]$  for some mean distance  $d_0$  and some grid size  $2\sigma_d$ . When applying our method, all points within this range are treated as being in the “same” location bin indexed by  $d_0$ . By discretizing the location this way, we can reduce the number of locations indexed in the database and also provide resilience to errors in position information estimated by the vehicle. The edge effect can be avoided by defining overlapping location bins.

The output from the ray-tracing simulation is combined with the geometric channel model to obtain the corresponding channel matrix. A ray-tracing simulation outputs a number of rays, each corresponding to a distinct propagation path. The information associated with each ray includes the received power, the delay of the path, the phase, the AoA, and the AoD. Denoting  $(\cdot)^*$  the conjugate transpose,  $N_t$  and  $N_r$  the numbers of transmit and receive antennas,  $L_p$  the number of rays,  $\alpha_{\ell}$  the channel gain,  $\beta_{\ell}$  the phase,  $\tau_{\ell}$  the delay,  $\theta_{\ell}^A$  and  $\theta_{\ell}^D$  the elevation AoA and AoD,  $\varphi_{\ell}^A$  and  $\varphi_{\ell}^D$  the azimuth AoA and AoD of the  $\ell$ -th ray,  $g(\cdot)$  the combined effect of lowpass

filtering and pulse shaping,  $T$  the symbol period, and  $\mathbf{a}_r(\cdot)$  and  $\mathbf{a}_t(\cdot)$  the receive and transmit steering vectors, the channel can be written as

$$\mathbf{H}[n] = \sqrt{N_r N_t} \sum_{\ell=0}^{L_p-1} \alpha_{\ell} e^{j\beta_{\ell}} g(nT - \tau_{\ell}) \mathbf{a}_r(\theta_{\ell}^A, \varphi_{\ell}^A) \mathbf{a}_t^*(\theta_{\ell}^D, \varphi_{\ell}^D), \quad (2)$$

The raised cosine filter with a roll-off factor of 0.1 is assumed for the pulse shaping filter. We use uniform planar arrays (UPAs) at both the transmitter and the receiver. Let  $\Omega_y = k d_y \sin(\theta) \sin(\varphi)$ ,  $\Omega_x = k d_x \sin(\theta) \cos(\varphi)$ ,  $k = 2\pi/\lambda$  be the wave number,  $\otimes$  denote the Kronecker product,  $N_x$  and  $N_y$  be the numbers of elements along the x- and y-axis, and  $d_x$  and  $d_y$  be the element spacing in the x- and y-direction, the steering vector is

$$\mathbf{a}(\theta, \varphi) = \frac{1}{\sqrt{N_x N_y}} \begin{bmatrix} 1 \\ e^{j\Omega_y} \\ \vdots \\ e^{j(N_y-1)\Omega_y} \end{bmatrix} \otimes \begin{bmatrix} 1 \\ e^{j\Omega_x} \\ \vdots \\ e^{j(N_x-1)\Omega_x} \end{bmatrix}.$$

In this paper, we use  $d_x = d_y = \lambda/2$ .

### B. Received Signal Model

We consider an analog beamforming architecture, where there is only one RF chain. Assuming that the symbol timing is synchronized to the first path (shortest delay), the received signal when the  $i$ -th beam pair is used can be written as

$$y_i[k] = \sqrt{P_t} \sum_{n=0}^{L-1} s[k-n] \underbrace{\sum_{\ell=0}^{L_p-1} g(nT + \tau_0 - \tau_{\ell}) \mathbf{w}_{r(i)}^* \mathbf{H}_{\ell} \mathbf{f}_{t(i)} + v_i[k]}_{h_i[n]}, \quad (3)$$

where  $\mathbf{H}_{\ell} = \sqrt{N_r N_t} \alpha_{\ell} e^{j\beta_{\ell}} \mathbf{a}_r(\theta_{\ell}^A, \varphi_{\ell}^A) \mathbf{a}_t^*(\theta_{\ell}^D, \varphi_{\ell}^D)$ ,  $P_t$  is the transmit power,  $s[k]$  is the known training signal,  $r(i)$  and  $t(i)$  denote the mapping of the beam pair index  $i$  to the combiner and beamformer vector indices, and  $v_i[k]$  is the zero mean complex Gaussian noise  $\mathcal{CN}(0, \sigma_v^2)$ . Let  $\mathbf{S}$  be the  $K \times L$  matrix of circularly shifted training sequence of length  $K \geq L$ , the channel  $\mathbf{h}_i = [h_i[0] \ h_i[1] \ \dots \ h_i[L-1]]^T$  can be estimated using a least-square approach as

$$\hat{\mathbf{h}}_i = \mathbf{S}^{\dagger} \mathbf{y}_i \quad (4)$$

$$= \mathbf{h}_i + \mathbf{S}^{\dagger} \mathbf{v}_i \quad (5)$$

where  $\mathbf{y}_i = [y_i[0] \ h_i[1] \ \dots \ y_i[L-1]]^T$ ,  $\mathbf{v}_i = [v_i[0] \ v_i[1] \ \dots \ v_i[L-1]]^T$  and  $\mathbf{S}^{\dagger} = (\mathbf{S}^* \mathbf{S})^{-1} \mathbf{S}^*$  is the pseudo-inverse. When using a training sequence with good autocorrelation properties like Zadoff-Chu or Golay sequences,  $\mathbf{S}^* \mathbf{S} = K \mathbf{I}$  and the estimation error  $\tilde{\mathbf{v}}_i = \mathbf{S}^{\dagger} \mathbf{v}_i$  can be modeled as  $\mathcal{CN}(\mathbf{0}, \frac{\sigma_v^2}{K} \mathbf{I})$  [31]. Note that the received powers in the fingerprints have to be measured using the same  $P_t$  (or scaled appropriately if different measurements use different  $P_t$ ). We assume  $P_t = 0$  dBm when collecting the fingerprints and the received power is estimated as the squared norm of the

estimated channel  $\|\hat{\mathbf{h}}_i\|^2$ . In our simulations, we use  $K = 512$ . The actual channel length  $L$  varies for different snapshots of the ray-tracing simulation and can be larger than 512. Since the powers of those paths with large delays are observed to be negligible compared to paths with short delays, we truncate the channel to get  $L = 512$ .

The vector  $\mathbf{w}_{r(i)}$  and  $\mathbf{f}_{t(i)}$  are selected from the receiver codebook  $\mathcal{W}$  and transmitter codebook  $\mathcal{F}$ , respectively. We assume UPAs are used at both the CV and the RSU. The codebook is generated such that beams are separated by their 3dB-beamwidth. This ensures that the array gain fluctuates less than 3 dB over the entire field of view of the antenna array. We note that our proposed approach does not depend on this specific codebook, and any other codebook designs can replace the one used here.

### III. INVERSE FINGERPRINT BEAM ALIGNMENT

The main idea of the proposed approach is to leverage prior knowledge of the channel to efficiently perform beam alignment. The approach is inspired by the multipath fingerprint based localization methods, where the correlation between locations and fingerprints (i.e., the channel characteristics) is exploited. Such localization approaches rely on a fingerprint database that is indexed by locations. We proposed to use this idea in inverse, where the position of the CV is used to query the fingerprint database to identify beam directions that could provide strong link connections between the CV and RSU. Note that the information in the database is obtained from past observations, and some of these links may not exist in the current channel due to blockage by a truck for example. Therefore, beam training among the beam directions identified from the database is still required. The beam training here has much lower overhead than conventional methods because a large number of unlikely directions have already been eliminated using the database. In the following, we will define fingerprints and explain how the database is constructed. Then, we will describe the proposed approach for beam alignment.

#### A. Multipath Fingerprint Database

In general, a fingerprint refers to some characteristics of the channel at a given location. These characteristics could be the received signal strengths from different access points [7] or the multipath signature of the channel from an access point [8]. In this work, a fingerprint refers to a set of received signal powers observed via different pairs of transmit and receive beamformers at a given location. We note that the location here refers to a grid  $[d_0 - \sigma_d, d_0 + \sigma_d]$  so that the system can tolerate position information error used to query the fingerprint database. In our simulation, the grid size is set to 5 m, i.e.,  $\sigma_d = 2.5$  m.

We define three types of fingerprints, which differ by how measurement data are collected and stored. The first type, called Type A, requires that the set of received powers of all transmit and receive beam combinations are collected within a channel coherence time so that the spatial channel does not change, e.g., by having the contributing CV perform an exhaustive search. This way, the fingerprint captures the

correlation between the different beam pairs. For Type A fingerprints, the raw measurement samples are stored. An example of Type A fingerprints is shown in Table I. In this example, there are  $N$  observations of the received power for each beam pair. Fingerprint Type B and C relax the constraint requiring that the measurement of all the beam pair combinations be completed within a channel coherence time. This less restrictive measurement collection reduces the burden on vehicles contributing to building the fingerprint database, as they do not need to commit to conducting a full scan of the exhaustive search and could contribute as many beam measurements as their time allows. The disadvantage is that now the correlation between the beam pairs cannot be easily captured. While they share the same data collection condition, these two types differ in how they store the measurements. Type B fingerprints store the raw samples directly in the same manner as Type A fingerprints. Type B fingerprints look similar to that of Type A fingerprints, but now it is not required that all the measurements in a column in Table I be collected within a channel coherence time and that each row could have a different number of entries. Type C fingerprints assume the same data collection as that of Type B but store statistical summaries instead of the raw samples to save data storage requirement. An example of Type C fingerprints is shown in Table II.

To statistically summarize the raw observations for Type C fingerprints, the received power (in linear scale) observed at a given beam pair (each row in Table I) is modeled by the Gaussian distribution because it is observed to provide a good fit to the data once the observations with low received powers are removed. Note that the low received power could be due to blockage, path disappearance (e.g., paths via reflections off neighboring vehicles, which exist only if there is a vehicle in certain locations), or some other reason. We collectively call these cases blocked for convenience. We introduce a simple rule to identify blockage by defining a threshold  $\Gamma_{\text{th}}$ , and classify those observations whose received powers are  $\Gamma_{\text{th}}$  lower than the observed peak power as blocked. In our numerical results, we set  $\Gamma_{\text{th}} = 20$  dB. Since the Gaussian distribution is fully described by its mean and variance, we can summarize the observations of each beam pair by three parameters, namely, the mean, the standard deviation, and the blockage probability. The fingerprint after the statistical summary is illustrated in Table II.

We consider an offline learning approach to build the database in this work. The idea can readily be implemented online in practice, especially for Type B and C fingerprints. In the proposed approach, the database is built and maintained by the RSU. By offline learning, we mean there is a dedicated period of time that is used to collect data to build the fingerprint database before it is exploited for efficient beam alignment. During this period, we assume that each contributing vehicle conducts beam training with the RSU. By having the vehicle be the transmitter during the beam training, there is no feedback. The RSU can measure the received power for each of the beam pairs and collect these observations to build the fingerprint database. In the case that each contributing vehicle can perform a full exhaustive search

TABLE I  
AN EXAMPLE OF TYPE A FINGERPRINTS. TYPE B FINGERPRINTS ARE SIMILAR, BUT EACH ROW, WHICH CORRESPONDS TO THE NUMBER OF MEASUREMENTS FOR A GIVEN BEAM PAIR, COULD HAVE A DIFFERENT NUMBER OF COLUMNS.

Tx beam index	Rx beam index	Observation 1	Observation 2	...	Observation $N$
92	258	-70.4 dBm	-68.1 dBm	...	-64.5 dBm
1	262	-72.6 dBm	-66.4 dBm	...	-84.3 dBm
...	...	...	...	...	...

TABLE II  
AN EXAMPLE OF TYPE C FINGERPRINTS AT A GIVEN LOCATION.

Tx beam index	Rx beam index	Mean	Std deviation	Blockage probability
92	258	-66.9 dBm	-71.0 dBm	0.52
1	262	-73.5 dBm	-73.1 dBm	0.30
...	...	...	...	...

over all beam pair combinations in the codebook, we obtain Type A fingerprints that can capture the correlations between the different beam pairs. Otherwise, we obtain Type B or Type C fingerprints depending on how we store the measurement data. A possible approach for implementing the online learning is to divide the training period of each contributing vehicle into two parts, where one is dedicated to building the database and the other to performing the beam alignment using the currently available fingerprint database to find a good path for its communication needs. How to balance between these two parts is a good subject for future work.

### B. Proposed Beam Alignment

Fig. 2 shows how the proposed beam alignment works. The procedure is initiated by a CV by transmitting a beam training request using a low frequency system such as DSRC or mmWave communication with a large spreading factor. Within this request packet, the CV also includes its current position, which is available from some localization sensors equipped on the vehicle (e.g., GPS or other more advanced positioning method based on LIDAR and 3D map [9]). Upon receiving the request, the RSU will use the position information to query its database to obtain the fingerprint associated with that location. Using the fingerprint, the RSU determines the candidate beam pairs that are likely to provide a satisfactory link connection. The RSU then responds back with an acknowledgment to allow the beam training and also provides a list of candidate beams. Several methods to select the candidate beams will be described in Section V after the analysis in Section IV, which provides a framework for optimizing the choice of the candidate beams. The CV can now proceed to perform the beam training following the list provided by the RSU. Upon completing the list, the RSU provides a feedback indicating the best beam index to the CV. This feedback ends the beam alignment and high data rate mmWave communication can start.

Several remarks on the details of the proposed approach are now provided.

*Remark 1:* The position information here does not have to be highly accurate. It only needs to be accurate enough to identify the location bin index of the fingerprints. In our simulation,

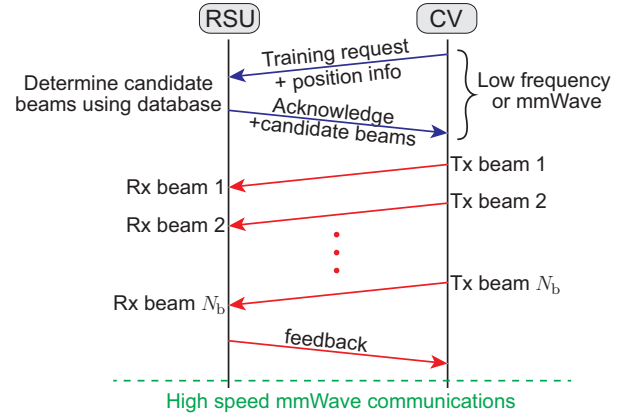


Fig. 2. Timing diagram of the proposed inverse fingerprint beam alignment method. The CV sends beam training request along with its position to the RSU. The RSU would acknowledge and provide a list of candidate beam pairs for training by querying the fingerprint database using the CV's position. Beam training can then start following the list. At the end, the RSU feedbacks to best observed beam to the CV and high speed mmWave communications can begin.

this bin size is 5 m. Edge effects can be avoided by having overlapping location bins.

*Remark 2:* The proposed method allows graceful degradation as the number of beam pairs trained  $N_b$  decreases because the alignment accuracy decreases probabilistically with  $N_b$  and there is no hard threshold on  $N_b$ . See Fig. 7(a) for an example of how the average rate changes with  $N_b$ . This is a desirable feature that allows the tradeoff between latency in link establishment and accuracy of the beam alignment.

*Remark 3:* Our method performs the beam training using only narrow beams, which provides several advantages. Narrow beams provide high antenna gain, are more resilient to Doppler spread [11], and do not require large spreading factors during the beam training as in conventional beam sweeping methods. For example, IEEE 802.11ad uses  $32\times$  spreading during the initial sector level sweep. Also, methods employing wide quasi-omni beams can suffer from antenna gain fluctuation because it is challenging to realize wide beamwidths with low gain fluctuation [15].

*Remark 4:* By having the CV transmit and the RSU receive during the beam training, the RSU can obtain observations

of different beam pairs for free, i.e., without any feedback from the CV. Although outside the scope of this work, these observations during the beam training can be used to update the fingerprint database.

#### IV. QUANTIFYING BEAM ALIGNMENT ACCURACY USING FINGERPRINT

This section provides analysis for measuring the beam alignment accuracy using the information available in the fingerprint. The analysis allows us to compare different candidate beam selection methods and can be used as a framework for optimizing the method to select candidate beams for training in Section V. We define the power loss probability as the performance metric and derive an expression to compute this probability using the information in the fingerprints ignoring the measurement noise (i.e., the noise term  $v$  in (3) is neglected). The effect of noise will be investigated numerically in Section VI-C.

The power loss is defined as the ratio between the received power of the optimal beam pair and the pair selected by the proposed beam alignment solution indexed by  $s$ . Let  $\mathcal{B}$  be the set of all beam pairs in the fingerprint, and  $\gamma_\ell = \|\mathbf{h}_\ell\|^2$  be the received power of the  $\ell$ -th beam pair. The power loss can be written as

$$\xi = \frac{\max_{k \in \mathcal{B}} \gamma_k}{\gamma_s}. \quad (6)$$

If noise is negligible, the strongest beam pair will be selected after the beam training so that  $\gamma_s = \max_{i \in \mathcal{S}} \gamma_i$ , where  $\mathcal{S} \subset \mathcal{B}$  is the set of candidate beams selected for beam training. The power loss probability is defined as the probability that  $\xi > c$  for some  $c \geq 1$ , i.e.,

$$P_{\text{pl}}(c, \mathcal{S}) = \mathbb{P}[\xi > c] \quad (7)$$

$$= \mathbb{P} \left[ \max_{k \in \mathcal{B} \setminus \mathcal{S}} \gamma_k > c \max_{i \in \mathcal{S}} \gamma_i \right]. \quad (8)$$

We note that the event  $\{\max_{k \in \mathcal{B}} \gamma_k > c \max_{i \in \mathcal{S}} \gamma_i\}$  is equivalent to  $\{\max_{k \in \mathcal{B} \setminus \mathcal{S}} \gamma_k > c \max_{i \in \mathcal{S}} \gamma_i\}$  because if the maximum pair is not in  $\mathcal{S}$  then  $\max_{k \in \mathcal{B}} \gamma_k = \max_{k \in \mathcal{B} \setminus \mathcal{S}} \gamma_k$  and if the maximum pair is in  $\mathcal{S}$  then both events are false. Using  $\mathcal{B} \setminus \mathcal{S}$  instead of  $\mathcal{B}$  helps in later derivations because  $\mathcal{B} \setminus \mathcal{S}$  and  $\mathcal{S}$  are disjoint.

In the following, we derive formulas to compute  $P_{\text{pl}}(c, \mathcal{S})$  using the three types of fingerprints, which will be leveraged in Section V in designing candidate beam pair selection methods.

##### A. $P_{\text{pl}}(c, \mathcal{S})$ Using Type A Fingerprints

Type A fingerprints are collected via exhaustive search by each contributing vehicle. Here we assume the received powers in a column in Table I were collected within a channel coherence time so that the correlation between the beam pairs is captured in the fingerprint. To exploit the correlation, a Monte Carlo approximation of the power loss probability is computed using the observations in the fingerprint directly. Denote  $\gamma_{kn}$  the received power observed at the  $k$ -th beam pair in the  $n$ -th observation,  $P_{\text{pl}}(c, \mathcal{S})$  is given by

$$P_{\text{pl}}(c, \mathcal{S}) \simeq \frac{1}{N} \sum_{n=1}^N \mathbf{1} \left\{ \max_{k \in \mathcal{B} \setminus \mathcal{S}} \gamma_{kn} > c \max_{i \in \mathcal{S}} \gamma_{in} \right\} \quad (9)$$

where  $N$  is the number of observations in the fingerprint and  $\mathbf{1}\{E\}$  is the indicator function which outputs 1 if  $E$  is true and 0 otherwise. This approximation is guaranteed to converge to the true probability by the law of large numbers [32]. Because of the sparsity of the mmWave channel, we expect that only a small subset of the beam pairs in  $\mathcal{B}$  has significant contribution so that the approximation is meaningful even with a relatively small  $N$ . In Section VI-A, we use  $N = 450$  although a smaller number can still work (see Section VI-B).

##### B. $P_{\text{pl}}(c, \mathcal{S})$ Using Type B Fingerprints

Here we use the raw observations directly as when using Type A fingerprints but we do not require that each column in Table I be collected within a channel coherence time. This way, a contributing vehicle can perform any amount of beam training (i.e., not necessarily a full exhaustive search) within its time budget, and this approach is more amenable to online database building as remarked in Section III-B. We note that in this case, the numbers of observations for two different pairs do not have to be the same, i.e., the number of entries at each row in Table I could be different.

The power loss probability can be computed as shown in (10) to (13), where  $N_\ell$  is the number of received powers at the  $\ell$ -th pair, and  $\gamma_{\ell n}$  denotes the  $n$ -th observed received power at the  $\ell$ -th beam pair in the fingerprint. The first step follows from the law of total probability on the event  $\{\ell = \arg \max_{k \in \mathcal{B} \setminus \mathcal{S}} \gamma_k\}$ , (11) is by conditioning on  $\gamma_\ell$ , (12) follows from the independence assumption of different pairs (because Type B fingerprints do not have correlation information), and (13) is the result of applying Monte Carlo approximation. One main benefit of using the raw samples directly is that we do not need to know an explicit distribution of the received powers and thus can avoid modeling mismatch.

##### C. $P_{\text{pl}}(c, \mathcal{S})$ Using Type C Fingerprints

Different from Type B fingerprints, now we have the statistical summaries of the samples rather than the raw samples as shown in Table II. As described in Section III-A, the received powers are observed to fit well with the Gaussian distribution once the blockage cases have been removed. More precisely, the received power of the  $k$ -th beam pair is assumed to follow a Bernoulli-Gaussian model as

$$\gamma_k = \begin{cases} 0 & \text{w.p. } P_k^{\text{blk}} \\ \sim \tilde{\mathcal{N}}(\mu_k, \sigma_k^2) & \text{w.p. } 1 - P_k^{\text{blk}} \end{cases}, \quad (14)$$

where we interpret “being blocked” to mean  $\gamma_k = 0$ ,  $P_k^{\text{blk}}$  denotes the blockage probability, and  $\tilde{\mathcal{N}}(\mu_k, \sigma_k^2)$  denotes the truncated Gaussian distribution with the mean  $\mu_k$  and the variance  $\sigma_k^2$  so that the received power is always non-negative.

The power loss probability can be derived in the same way as that for Type B fingerprints to get (12). Now, instead of using Monte Carlo approximations as in (13), we use the distribution of the received power to compute the expectation in (12). Using the model in (14), the probability terms in the expectation in (12) can be expressed as

$$\mathbb{P}[\gamma_k < a] = P_k^{\text{blk}} + \tilde{F}_k^{\text{blk}} F_k(a) \quad (15)$$

$$P_{\text{pl}}(c, \mathcal{S}) = \sum_{\ell \in \mathcal{B} \setminus \mathcal{S}} \mathbb{P} \left[ \max_{i \in \mathcal{S}} \gamma_i < \frac{1}{c} \gamma_\ell \mid \ell = \arg \max_{k \in \mathcal{B} \setminus \mathcal{S}} \gamma_k \right] \mathbb{P} \left[ \ell = \arg \max_{k \in \mathcal{B} \setminus \mathcal{S}} \gamma_k \right] \quad (10)$$

$$= \sum_{\ell \in \mathcal{B} \setminus \mathcal{S}} \mathbb{E}_{\gamma_\ell} \left[ \mathbb{P} \left[ \max_{i \in \mathcal{S}} \gamma_i < \frac{1}{c} \gamma_\ell \mid \ell = \arg \max_{k \in \mathcal{B} \setminus \mathcal{S}} \gamma_k, \gamma_\ell \right] \mathbb{P} \left[ \ell = \arg \max_{k \in \mathcal{B} \setminus \mathcal{S}} \gamma_k \mid \gamma_\ell \right] \right] \quad (11)$$

$$= \sum_{\ell \in \mathcal{B} \setminus \mathcal{S}} \mathbb{E}_{\gamma_\ell} \left[ \prod_{i \in \mathcal{S}} \mathbb{P} \left[ \gamma_i < \frac{1}{c} \gamma_\ell \mid \gamma_\ell \right] \cdot \prod_{k \in \mathcal{B} \setminus \mathcal{S}, k \neq \ell} \mathbb{P} [\gamma_k < \gamma_\ell \mid \gamma_\ell] \right] \quad (12)$$

$$\simeq \sum_{\ell \in \mathcal{B} \setminus \mathcal{S}} \frac{1}{N_\ell} \sum_{n=1}^{N_\ell} \prod_{i \in \mathcal{S}} \frac{1}{N_i} \sum_{m=1}^{N_i} \mathbf{1} \left\{ \gamma_{im} < \frac{1}{c} \gamma_{\ell n} \right\} \prod_{k \in \mathcal{B} \setminus \mathcal{S}, k \neq \ell} \frac{1}{N_k} \sum_{u=1}^{N_k} \mathbf{1} \{ \gamma_{ku} < \gamma_{\ell n} \}, \quad (13)$$

$$P_{\text{pl}}(c, \mathcal{S}) = \sum_{\ell \in \mathcal{B} \setminus \mathcal{S}} \tilde{P}_\ell^{\text{blk}} \tilde{\mathbb{E}}_{\gamma_\ell} \left[ \prod_{i \in \mathcal{S}} \left( P_i^{\text{blk}} + \tilde{P}_i^{\text{blk}} F_i(\gamma_\ell/c) \right) \prod_{k \in \mathcal{B} \setminus \mathcal{S}, k \neq \ell} \left( P_k^{\text{blk}} + \tilde{P}_k^{\text{blk}} F_k(\gamma_\ell) \right) \right] \\ + \sum_{\ell \in \mathcal{B} \setminus \mathcal{S}} P_\ell^{\text{blk}} \prod_{i \in \mathcal{S}} (P_i^{\text{blk}}) \prod_{k \in \mathcal{B} \setminus \mathcal{S}, k \neq \ell} (P_k^{\text{blk}}) \quad (16)$$

$$\simeq \sum_{\ell \in \mathcal{B} \setminus \mathcal{S}} \tilde{P}_\ell^{\text{blk}} \tilde{\mathbb{E}}_{\gamma_\ell} \left[ \prod_{i \in \mathcal{S}} \left( P_i^{\text{blk}} + \tilde{P}_i^{\text{blk}} F_i(\gamma_\ell/c) \right) \prod_{k \in \mathcal{B} \setminus \mathcal{S}, k \neq \ell} \left( P_k^{\text{blk}} + \tilde{P}_k^{\text{blk}} F_k(\gamma_\ell) \right) \right] \quad (17)$$

where  $a > 0$  is some constant,  $\tilde{P}_k^{\text{blk}} = 1 - P_k^{\text{blk}}$ , and  $F_k(a)$  is the CDF of the truncated Gaussian distribution with the mean  $\mu_k$  and the variance  $\sigma_k^2$ . Substituting (15) into (12) and conditioning on whether  $\gamma_\ell$  is blocked or not, we have (16), where  $\tilde{\mathbb{E}}_{\gamma_\ell}[\cdot]$  denotes the expectation over the truncated Gaussian distribution  $\tilde{\mathcal{N}}(\mu_\ell, \sigma_\ell^2)$ , i.e., when the  $\ell$ -th beam pair is not blocked, and we used the fact that  $F_k(0) = 0$  in the second term in (16). Note that the second term in (16) is the probability that all the beam pairs are blocked, which is unlikely and can be neglected to get (17).

## V. CANDIDATE BEAM PAIR SELECTION METHODS

This section proposes two methods to select candidate beam pairs for beam training using the information in the fingerprint database. The objective of the selection methods is to maximize the received power of the finally selected pair for a given beam training budget of  $N_b$ . The first approach is a heuristic, while the second one minimizes the misalignment probability derived in Section IV.

### A. Selection Based on Expected Received Power

This method is based on the simple intuition that we should choose candidate beam pairs with high expected received power. When using Type A or Type B fingerprints, this is the sample average over all the observations for that particular beam pair. When using Type C fingerprints, the expected received power of the  $i$ -th beam pair can be computed as

$$\bar{\gamma}_i = \tilde{P}_i^{\text{blk}} \mathbb{E}[\gamma_i | \text{blk}(i) = 0] + P_i^{\text{blk}} \mathbb{E}[\gamma_i | \text{blk}(i) = 1] \quad (18)$$

$$= \tilde{P}_i^{\text{blk}} \mu_i, \quad (19)$$

where  $\text{blk}(i) = 1$  denotes the  $i$ -th beam pair is blocked,  $\mathbb{E}[\gamma_i | \text{blk}(i) = 0] = \mu_i$  as defined in (14), and we assumed that the received power is negligible when blocked, i.e.,  $\mathbb{E}[\gamma_i | \text{blk}(i) = 1] = 0$ . The proposed approach is to first rank the beam pairs by their expected received power  $\bar{\gamma}_i$  in descending order and select the highest  $N_b$  pairs for beam training. Note that this metric balances the blockage probability and the average power when not blocked. As a result, opportunistic paths that have larger blockage probability but high averaged power when not blocked will have relatively high expected averaged power and will likely be selected for beam training. Note that this method produces the same selection set for all the three types of fingerprints.

### B. Selection Based on Minimizing the Misalignment Probability

Since the objective of beam alignment is to maximize the received power, an indirect way to achieve that is to choose the beam pair to minimize the misalignment probability, which is the power loss probability  $P_{\text{pl}}(c = 1, \mathcal{S})$ . For a given training budget of  $N_b$ , the problem can be formulated as a subset selection problem given by

$$\begin{aligned} & \underset{\mathcal{S} \subset \mathcal{B}}{\text{minimize}} && P_{\text{pl}}(1, \mathcal{S}) \\ & \text{subject to} && |\mathcal{S}| = N_b \end{aligned} \quad (20)$$

Here  $|\mathcal{S}|$  denotes the cardinality of the set  $\mathcal{S}$ . This is a subset selection problem, which is combinatoric in nature and is difficult to solve in general especially when  $|\mathcal{B}|$  is large. Fortunately, the structure of  $P_{\text{pl}}(1, \mathcal{S})$  allows an efficient solution. Note that the problem (20) is equivalent to maximizing  $\bar{P}_{\text{pl}}(1, \mathcal{S}) = 1 - P_{\text{pl}}(1, \mathcal{S})$ . Since  $\bar{P}_{\text{pl}}(1, \mathcal{S})$  is a

modular function, the greedy solution given in Algorithm 1 is optimal [33, Theorem 7]. This is a well-known result that has been reported in different forms in the literature (see [34] and references therein).

---

**Algorithm 1** Greedy candidate beam pair selection
 

---

```

1:  $\mathcal{S}_0 \leftarrow \emptyset$ 
2: for  $n = 1 : N_b$  do
3:    $\mathcal{S}_n \leftarrow \mathcal{S}_{n-1} \cup \arg \min_{i \in \mathcal{B} \setminus \mathcal{S}_{n-1}} P_{\text{pl}}(1, \mathcal{S}_{n-1} \cup \{i\})$ 
4: end for
  
```

---

*Claim 1:*  $\bar{P}_{\text{pl}}(1, \mathcal{S})$  is modular.

*Proof:* Using the definition of power loss probability in (7) with  $c = 1$ , we have

$$P_{\text{pl}}(1, \mathcal{S}) = \mathbb{P} \left[ \max_{k \in \mathcal{B}} \gamma_k > \max_{i \in \mathcal{S}} \gamma_i \right] \quad (21)$$

$$= \sum_{\ell \in \mathcal{B}} \mathbb{P} \left[ \gamma_\ell > \max_{i \in \mathcal{S}} \gamma_i \mid \gamma_\ell = \max_{k \in \mathcal{B}} \gamma_k \right] \mathbb{P} \left[ \gamma_\ell = \max_{k \in \mathcal{B}} \gamma_k \right] \quad (22)$$

$$= \sum_{\ell \in \mathcal{B} \setminus \mathcal{S}} \mathbb{P} \left[ \gamma_\ell = \max_{k \in \mathcal{B}} \gamma_k \right] \quad (23)$$

$$= 1 - \sum_{\ell \in \mathcal{S}} \mathbb{P} \left[ \gamma_\ell = \max_{k \in \mathcal{B}} \gamma_k \right], \quad (24)$$

where (22) is the application of the law of total probability on the event  $\{\gamma_\ell = \max_{k \in \mathcal{B}} \gamma_k\}$ , and (23) follows because if  $\ell \in \mathcal{S}$  then  $\mathbb{P}[\gamma_\ell > \max_{i \in \mathcal{S}} \gamma_i \mid \gamma_\ell = \max_{k \in \mathcal{B}} \gamma_k] = 0$  and if  $\ell \in \mathcal{B} \setminus \mathcal{S}$  then  $\mathbb{P}[\gamma_\ell > \max_{i \in \mathcal{S}} \gamma_i \mid \gamma_\ell = \max_{k \in \mathcal{B}} \gamma_k] = 1$ . Using the fact that  $\sum_{\ell \in \mathcal{B}} \mathbb{P}[\gamma_\ell = \max_{k \in \mathcal{B}} \gamma_k] = 1$ , we obtain (24). From (24), we have

$$\bar{P}_{\text{pl}}(1, \mathcal{S}) = \sum_{\ell \in \mathcal{S}} \mathbb{P} \left[ \gamma_\ell = \max_{k \in \mathcal{B}} \gamma_k \right]. \quad (25)$$

Thus, for any  $\mathcal{S} \subset \mathcal{T} \subset \mathcal{B}$  and  $\forall n \in \mathcal{B} \setminus \mathcal{T}$ , we have  $\bar{P}_{\text{pl}}(1, \mathcal{S} \cup \{n\}) - \bar{P}_{\text{pl}}(1, \mathcal{S}) = \bar{P}_{\text{pl}}(1, \mathcal{T} \cup \{n\}) - \bar{P}_{\text{pl}}(1, \mathcal{T}) = \mathbb{P}[\gamma_n = \max_{k \in \mathcal{B}} \gamma_k]$ , which is the definition of modular functions [34], [35]. ■

While the solution in Algorithm 1 is intuitive, using a brute force search to solve the minimization problem at each selection step has high complexity. At each selection step, we need to evaluate the power loss probability  $|\mathcal{B} \setminus \mathcal{S}_{n-1}|$  times. Since  $|\mathcal{B}|$  typically is much larger than  $N_b$ , this means that the total number of evaluations is  $\mathcal{O}(|\mathcal{B}|^2)$ . Defining the probability of being optimal as

$$P_{\text{opt}}(i) = \mathbb{P} \left[ \gamma_i = \max_{k \in \mathcal{B}} \gamma_k \right] \quad (26)$$

$$= \mathbb{P}[\gamma_i \geq \gamma_k, \forall k \in \mathcal{B} \setminus \{i\}], \quad (27)$$

the proof above suggests a more efficient solution. Observing (24), we see that minimizing  $P_{\text{pl}}(1, \mathcal{S}_{n-1} \cup \{i\})$  over  $i \in \mathcal{B} \setminus \mathcal{S}_{n-1}$  is equivalent to solving  $k = \arg \max_{i \in \mathcal{B} \setminus \mathcal{S}_{n-1}} P_{\text{opt}}(i)$ . This means that Algorithm 1 is equivalent to selecting the beam pairs by their probability of being optimal in descending order.

TABLE III  
COMMON SIMULATION PARAMETERS

Parameters	Value
Carrier frequency	60 GHz
Bandwidth	1760 MHz
Antenna array	16×16 UPA
Mean vehicle gap	4.78 m

We now present how to compute  $P_{\text{opt}}(i)$  using the different types of fingerprints. For Type A, this can be computed by

$$P_{\text{opt}}(i) \simeq \frac{1}{N} \sum_{n=1}^N \mathbf{1} \{ \gamma_{in} > \gamma_{kn}, \forall k \in \mathcal{B} \setminus \{i\} \}. \quad (28)$$

In the case of Type B, by assuming the independence between the pairs, this becomes

$$P_{\text{opt}}(i) = \mathbb{E}_{\gamma_i} \left[ \prod_{k \in \mathcal{B} \setminus \{i\}} \mathbb{P}[\gamma_i > \gamma_k | \gamma_i] \right] \quad (29)$$

$$\simeq \frac{1}{N_i} \sum_{n=1}^{N_i} \prod_{k \in \mathcal{B} \setminus \{i\}} \frac{1}{N_k} \sum_{m=1}^{N_k} \mathbf{1} \{ \gamma_{in} > \gamma_{km} \}. \quad (30)$$

When using the statistical summary of Type C, by conditioning on the blockage status of the  $i$ -th and  $k$ -th beam pairs this can be written as

$$P_{\text{opt}}(i) = \tilde{P}_i^{\text{blk}} \mathbb{E}_{\gamma_i} \left[ \prod_{k \in \mathcal{B} \setminus \{i\}} (P_k^{\text{blk}+} \tilde{P}_k^{\text{blk}} \mathbb{P}[\gamma_i > \gamma_k | \gamma_i, \text{blk}(i, k) = 0]) \right], \quad (31)$$

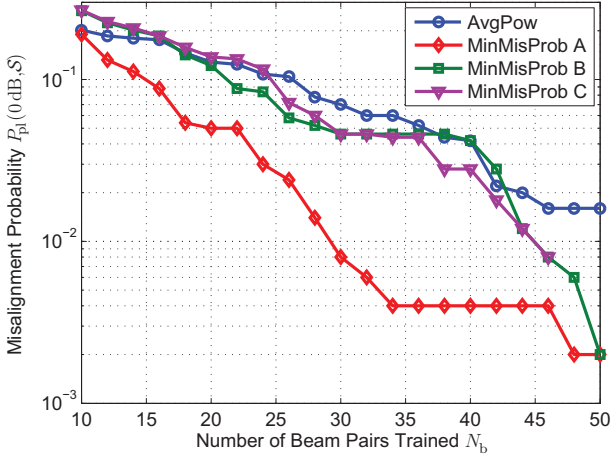
$$= \tilde{P}_i^{\text{blk}} \tilde{\mathbb{E}}_{\gamma_i} \left[ \prod_{k \in \mathcal{B} \setminus \{i\}} (P_k^{\text{blk}+} + \tilde{P}_k^{\text{blk}} F_k(\gamma_i)) \right], \quad (32)$$

where  $\text{blk}(i, k) = 0$  means both the  $i$ -th and  $k$ -th beam pairs are not blocked. Note that when using Type A, it is possible that the number of beam pairs with nonzero  $P_{\text{opt}}(\cdot)$  is smaller than the training budget  $N_b$ . In that case, we use the selection assuming Type B to fill in the selection set to reach  $N_b$ .

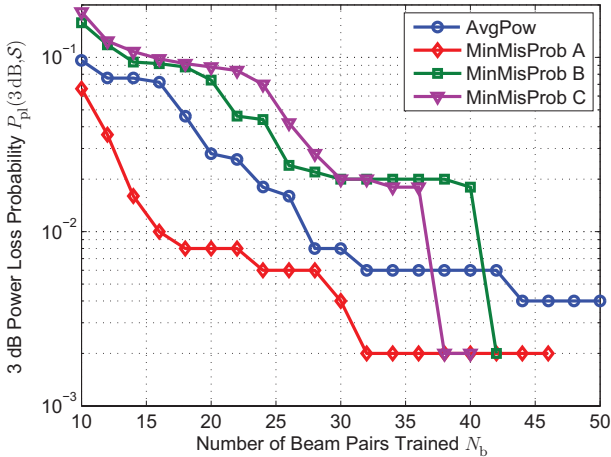
## VI. NUMERICAL RESULTS AND DISCUSSIONS

This section provides numerical evaluations of the proposed beam alignment. All evaluations here uses a dataset of 500 channel realizations generated from the ray-tracing simulator (see Fig. 1). All the results assume  $16 \times 16$  UPAs at both the CV and RSU unless specified otherwise. We conduct K-fold cross validation, with  $K = 10$  as recommended in [36]. Specifically, the dataset of 500 channel realizations is divided into 10 subsets (or folds) of size 50 each. Then, nine of them are used as the training set to build the database, and the remaining one is used as the test set to evaluate the proposed beam alignment. This is repeated 10 times, where each time a different subset is selected as the test data. When a different evaluation method is used, it will be stated explicitly. Common simulation parameters are summarized in Table III.





(a) Misalignment probability



(b) 3 dB power loss probability

Fig. 3. Power loss probability versus the number of beam pairs trained. Some of the plots end before reaching  $N_b = 50$  because there is no such instance of power loss computed from the cross validation. MinMisProb A outperforms other methods in both the misalignment and 3 dB power loss probability. AvgPow has comparable misalignment probability as MinMisProb B and MinMisProb C, but it performs better in terms of the 3 dB power loss probability. Thus, when Type A fingerprints are not available, AvgPow should be used.

#### A. Performance Comparison of Proposed Beam Pair Selection Methods

This subsection presents a performance comparison of the proposed beam alignment method with the different variants of beam pair candidate selection methods when measurement noise is negligible. The impact of noise will be considered in the next subsection. We consider four variants of the proposed candidate beam pair selections, namely, when using the selection by average received power (AvgPow method), and the selection by minimizing the misalignment probability using fingerprints of Type A, B, and C (called MinMisProb A, B, and C method, respectively). Recall that when using AvgPow, all three types of fingerprints yield the same result.

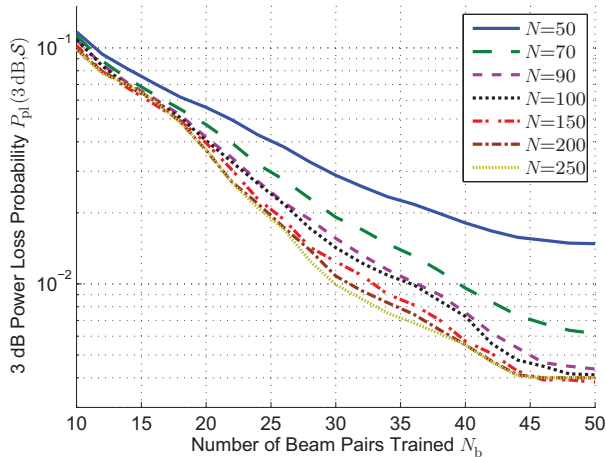
Fig. 3 compares the four variants of the beam pair selection methods in terms of power loss probability. Two different

levels of power loss severity are shown: the misalignment probability and the probability that the power loss is less than 3 dB (called the 3 dB power loss probability). MinMisProb A dominates other methods, because Type A fingerprints capture the correlation between the different beam pairs, and thus contain more information than the other two types of fingerprints. We note that when computing the probability of being optimal  $P_{\text{opt}}(\cdot)$  using Type A fingerprints, the number of pairs with nonzero  $P_{\text{opt}}(\cdot)$  could be small. In our dataset, this number is around 30 (the exact number depends on the folds chosen for training). For  $N_b$  larger than this value, we fill in by downgrading the fingerprints to Type B (i.e., ignoring the correlation between beam pairs) and we compute  $P_{\text{opt}}(\cdot)$  and select those that have not been selected. While the other three methods perform similarly in terms of the misalignment probability, the simpler AvgPow method performs better than the more sophisticated MinMisProb B and C method in terms of the 3 dB power loss probability. This is because by ignoring the correlation between the beam pairs, the prediction of  $P_{\text{opt}}(\cdot)$  using the fingerprint becomes inaccurate leading to poor selections. Note that while MinMisProb B and C method are slightly better than AvgPow for  $N_b$  of around 40 or larger, this translates to negligible differences in terms of average rate (see Fig. 7(a)). Therefore, if Type A fingerprints are available, MinMisProb A is the choice, otherwise the AvgPow method should be used.

#### B. Required Training Sample Size

This subsection provides an empirical evaluation to estimate the training sample size to build the fingerprint. By sample size here, we mean the number of columns of Table I denoted by  $N$ . We start with the description of the evaluation method. We still use the 10-fold cross validation as before, but now instead of using all the nine folds (450 samples) for training, we only use a subset of  $N < 450$  of these samples. To average out the dependence on the sampling of the subset, we repeat the evaluation of the test set 50 times, where in each time we randomly choose  $N$  samples out of the available training set of 450 samples to build the database. AvgPow is used as the selection method because it can be applied to all the three types of fingerprints.

We evaluate the quality of the fingerprint obtained using the training set of size  $N$  by the average power loss probability over the training subset sampling as mentioned above. Fig. 4 shows average 3 dB power loss probabilities for training sample size ranging from 50 to 250. We can see a large improvement when increasing  $N$  from 50 to 90. Subsequent increases in  $N$ , however, provide diminishing improvement. To see this effect more clearly, we plot in Fig. 4(b) the 3 dB power loss probability when the number of beam pairs trained is fixed at  $N_b = 30$ . This plot is typically known as the learning curve [36], which quantifies the improvement as the training sample size (i.e., the learning effort) increases. The figure shows the mean and the region of one standard deviation from the mean. We see a sharp improvement up to around  $N = 100$ , and a slower improvement beyond that. We thus conclude that training sample size of around 200 to 250 seems good enough.



(a) Average 3 dB power loss probability

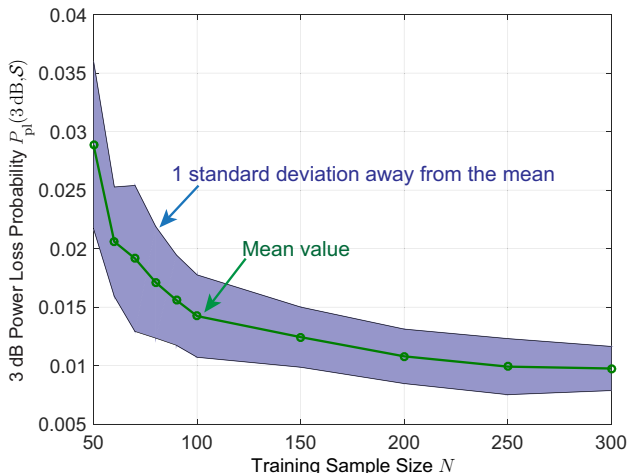
(b) Learning curve at  $N_b = 30$ 

Fig. 4. 3 dB power loss probability of AvgPow as a function of the training sample size  $N$ . Fig. 4(a) shows the average 3 dB power loss probability for different  $N$ . Fig. 4(b) shows the learning curve in terms of the 3 dB power loss probability when the number of beam pairs measured is set to  $N_b = 30$ . We can see from the plots that the improvement diminishes for subsequent increase in the training sample size.

### C. Effect of Measurement Noise

This subsection investigates the effect of measurement noise on the beam alignment accuracy. The results are shown in terms of the Equivalent Isotropic Radiated Power (EIRP), which is the transmit power plus the transmit antenna gain (in dB scale). EIRP is used instead of the transmit power because it is regulated [5]. To provide the context of the operating SNR, we start with a description of the link SNR of the channel generated from the ray-tracing simulation. As described earlier, the longitudinal distance of the CV from the RSU ranges in  $[27.5, 32.5]$  m, which translates to link distances in the range of  $[29.7, 34.3]$  m. We assume the noise power is given by  $P_n = -175 + 10 \log_{10} B$  dBm, where  $B = 1760$  MHz is the sampling rate defined in IEEE 802.11ad

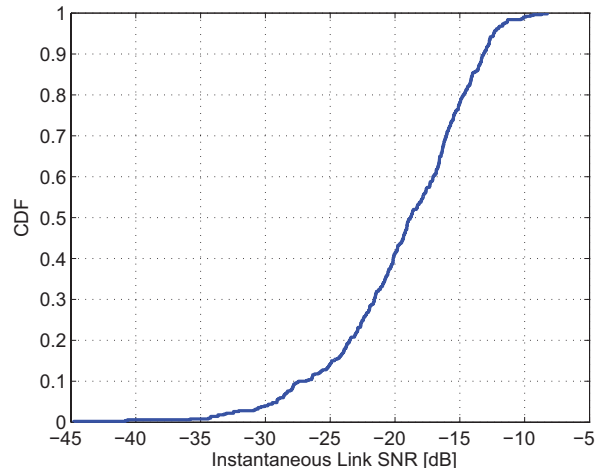


Fig. 5. CDF of the link SNR of the generated channels.

for single carrier PHY [28]. We define the link SNR by

$$\text{SNR} = \frac{P_0}{P_n}, \quad (33)$$

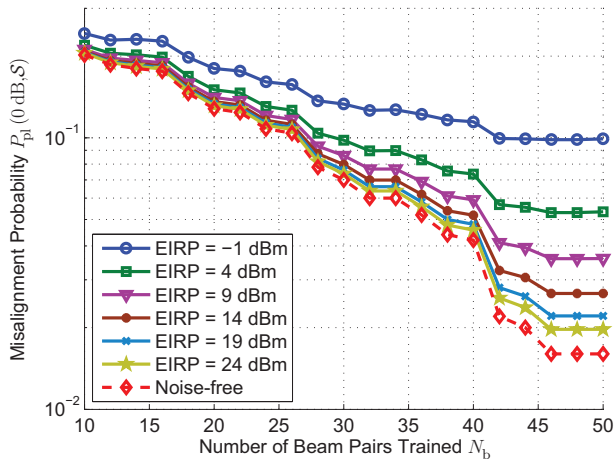
where  $P_0$  is the received power when isotropic antennas (0 dBi antenna gain) are used at both the transmitter and the receiver with 0 dBm transmit power. Fig. 5 shows the CDF of the link SNR computed from the received powers output from the ray-tracing simulation. We note that with an EIRP of 0 dBm, the SNR at the receiver is the link SNR.

Fig. 6 shows a comparison of the power loss probability with and without measurement noise when AvgPow is used. Other candidate selection methods show similar trends and are not shown here. We can see that the misalignment probability is much more affected than the 3 dB power loss probability. This is because for a 3 dB power loss event to happen the noise must be large enough to flip the order of the optimal pair with a beam pair that has the power of at least 3 dB below the optimal beam pair, which occurs much less frequent than the misalignment event (i.e., any non-zero power loss).

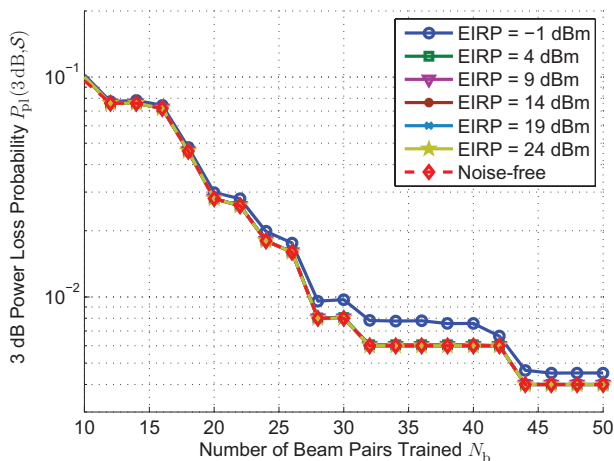
We show the average rates when using the proposed beam alignment in Fig. 7. The instantaneous rate is computed using

$$R_{\text{ins}} = \log_2 \left( 1 + \frac{P_t \|\mathbf{h}_s\|^2}{P_n} \right), \quad (34)$$

where  $\mathbf{h}_s$  is the effective channel of the beam pair selected after the beam training. Fig. 7(a) shows the average rate at a fixed EIRP of 24 dBm as a function of the number of beam pairs trained  $N_b$ . Increasing the training overhead  $N_b$  improves the alignment quality leading to higher average rates. The figure also compares the different beam pair candidate selection methods, which confirms the same trend as in the 3 dB power loss probability in Fig. 3(b). Fig. 7(b) shows the average rate as a function of EIRP for fixed  $N_b$ . At high EIRP, there is a non-diminishing gap when using a small  $N_b$ . This is because the power loss probability when using a small  $N_b$  is not negligible. In this result,  $N_b = 30$  provides accurate beam alignment with negligible average rate difference to the perfect alignment case.



(a) Misalignment probability with noise

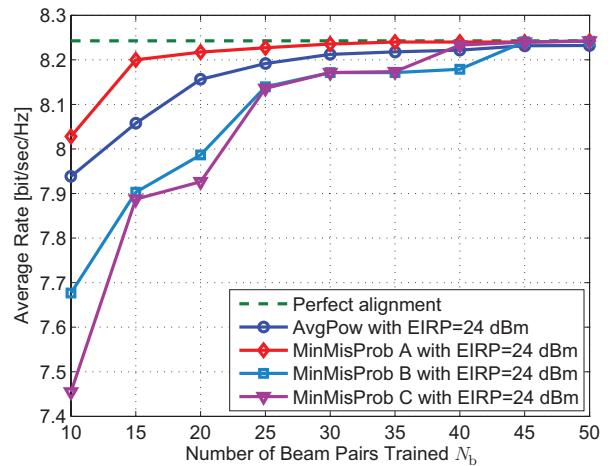
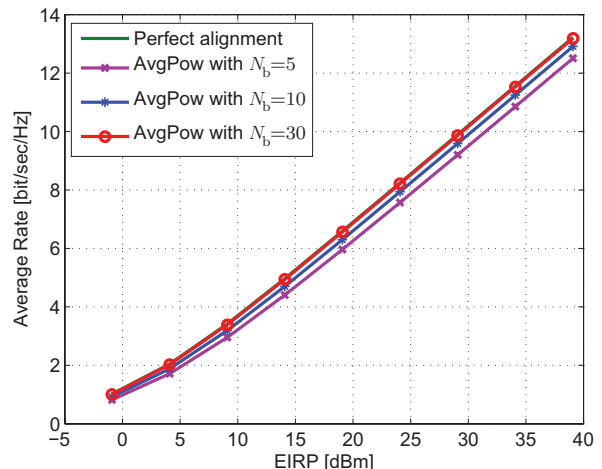


(b) 3 dB power loss probability with noise

Fig. 6. Power loss probability as a function of  $N_b$  in the presence of noise when using AvgPow selection method. The noise impacts the misalignment probability much more than the 3 dB power loss probability.

#### D. Overhead Comparison

This subsection compares the overhead of the proposed approach with IEEE 802.11ad as a baseline. IEEE 802.11ad beam alignment is a beam sweeping method using a hierarchical beam codebook structure to reduce the amount of beam training [15], [28]. It is required by the standard that the antenna gain of the quasi-omni pattern (the widest level in the codebook) be at most 15 dB ( $\approx 32$  in linear scale) lower than a directional pattern [28, Section 21.10.1]. Because of this constraint, we consider a two-level beam codebook: the quasi-omni and the sector level. We further assume for simplicity that the number of codewords at the sector level is equal to the number of elements of the array  $N_a$  (e.g., when using a 2D DFT codebook). Since the gain in the main beam direction of an array is  $N_a$ , we have  $N_{\text{sec}} = N_a$  and  $N_{\text{QO}} = N_{\text{sec}}/32$ , where  $N_{\text{sec}}$  is the number of sector beams and  $N_{\text{QO}}$  is the number of quasi-omni patterns. Since the quasi-omni patterns are the widest in the codebook, an exhaustive search is needed at the quasi-omni level to determine the best quasi-omni pair.

(a) Average rate as a function of  $N_b$ 

(b) Average rate as a function of EIRP when using AvgPow

Fig. 7. Average rate of the proposed beam alignment compared to the perfect alignment case.

The best sector is searched within the best quasi-omni pattern. To reduce the search complexity, IEEE 802.11ad uses the quasi-omni transmit pattern and sweeps through the sectors covered by the best quasi-omni receive pattern (called single-sided search). This process is repeated to find the best transmit sector. The total beam training time (excluding feedbacks) is then given by

$$T_{11ad} = N_{\text{QO}}^2 T_{\text{QO}} + 2 \frac{N_{\text{sec}}}{N_{\text{QO}}} T_{\text{sec}}, \quad (35)$$

where  $T_{\text{QO}}$  and  $T_{\text{sec}}$  are the duration of a training sequence at the quasi-omni and the sector level, respectively. The second term in (35) is based on the assumption that each quasi-omni pattern covers the same number of sectors. The factor two is because the single-sided search has to be conducted for both the transmitter and the receiver. We note that quasi-omni patterns have low antenna gain and thus require a large spreading factor to compensate for lack of antenna gain. IEEE 802.11ad uses  $32\times$  spreading for this. A beam training at the quasi-omni level is done by sending an SSW (sector

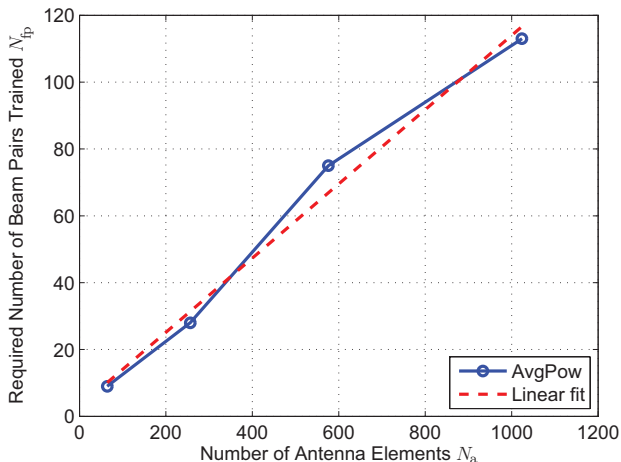


Fig. 8. Required amount of beam training of the proposed method. The overhead increases roughly linearly with the number of antenna elements of the array.

sweep) frame of length  $26.8 \mu\text{s}$ , which consists of  $4.3 \mu\text{s}$  for preamble and  $22.5 \mu\text{s}$  for header and information in the SSW frame. Since the preamble might be needed for synchronization purpose, we assume that it is unchanged and  $T_{\text{sec}} = 4.3 + 22.5/32 = 5.0 \mu\text{s}$ .

We now compute the overhead of the proposed approach. We define the overhead as the number of beam pairs trained  $N_{\text{fp}}$  needed to achieve  $P_{\text{pl}}(3 \text{ dB}, \mathcal{S}) \leq 1\%$ . Since our approach does not use wide beams for the beam training, we assume the training duration to be  $T_{\text{sec}}$ , and the total training time is

$$T_{\text{fp}} = N_{\text{fp}} T_{\text{sec}}. \quad (36)$$

Fig. 8 shows the required amount of beam training  $N_{\text{fp}}$  for UPAs of sizes  $8 \times 8$ ,  $16 \times 16$ ,  $24 \times 24$ , and  $32 \times 32$  when using AvgPow as the beam candidate selection method. The plot shows  $N_{\text{fp}}$  as a function of the number of elements  $N_a$ , which is roughly linear in  $N_a$ .

To understand this overhead in the mobility context, we leverage the concept of beam coherence time [11], which is the duration before beam realignment is required. The beam coherence time is the duration that the pointing error causes the received power to drop by some threshold from the peak. Since the codebook quantizes the angular domain by the 3-dB beamwidth, the initial pointing error ranges in  $[-\theta/2, \theta/2]$ , where  $\theta$  is the 3-dB beamwidth. Assuming the initial pointing error to be uniform in  $[-\theta/2, \theta/2]$ , then the beam coherence time is the duration that the pointing error becomes larger than half the 3-dB beamwidth. Using the pointing error derived in [11], the beam coherence time  $T_B$  can be written as

$$T_B = \frac{D}{v \sin \alpha} \frac{\theta}{2}, \quad (37)$$

where  $D$  is the distance to the reflector/scatterer,  $\alpha$  is the main beam direction with respect to the direction of travel, and  $v$  is the speed of the CV (see Fig. 9). We note that this result is based on a 2D model considering only the azimuth. This, however, is applicable here because there is negligible change in the elevation angle as the vehicle moves. Since we are

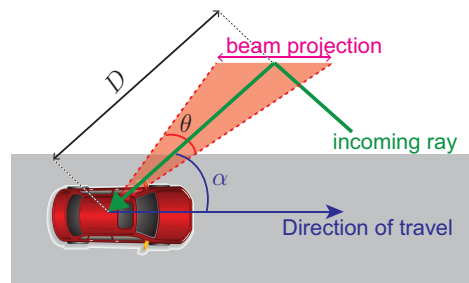


Fig. 9. An illustration of the beam coherence time concept. For the beam to stay aligned, the reflection point must be within the beam projection. The beam coherence time is the average time that the reflection point is within the beam projection.

considering a square array with total number of elements of  $N_a$ , the azimuth beamwidth  $\theta$  can be approximated by the beamwidth of a uniform linear array of size  $\sqrt{N_a}$  given by  $\theta \simeq 0.886 \frac{2}{\sqrt{N_a}}$  when the antenna spacing is set to half the wavelength [37, p. 885]. Using this approximation, we have

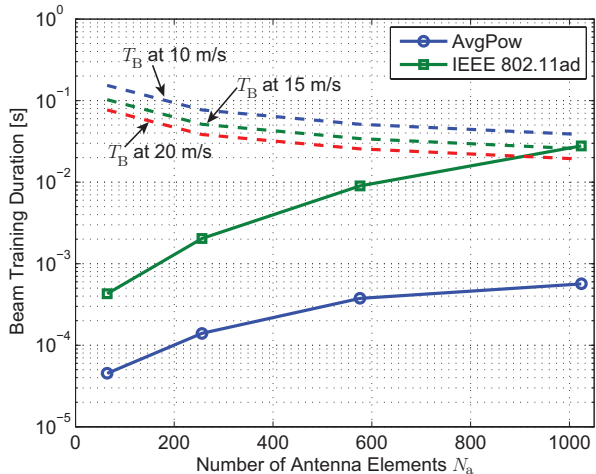
$$T_B(N_a) = \frac{0.886D}{v\sqrt{N_a} \sin \alpha}. \quad (38)$$

From the geometry, we set  $\alpha = 60^\circ$  and  $D = 12 \text{ m}$ , which represents reflections off the buildings in Fig. 1.

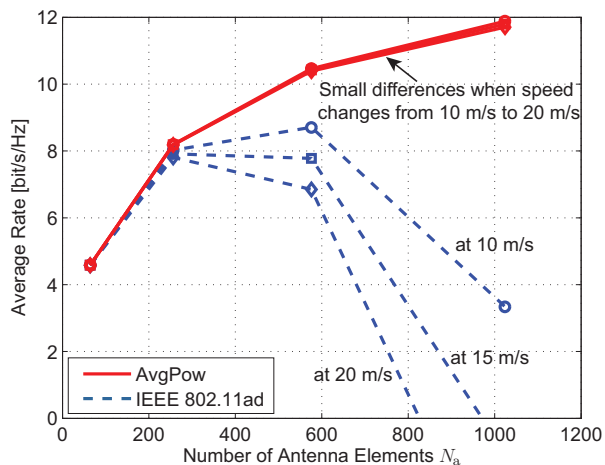
Fig. 10 compares the overhead of the proposed beam alignment using AvgPow selection method with that of IEEE 802.11ad. Fig. 10(a) shows beam training durations as a function of the array size  $N_a$ . We recall that this beam training duration does not include the initial training request and feedback, which do not depend on the array size. We also plot the beam coherence times  $T_B$  when the vehicle speed is 10, 15, and 20 m/s. The training duration of the proposed method is at most a few percents of  $T_B$ , while that of IEEE 802.11ad can exceed  $T_B$  when the array is large. This means that IEEE 802.11ad cannot finish the training before realignment is required. Fig. 10(b) compares the average rate when taking the beam training duration and  $T_B$  into account. The average rate here is defined as

$$R_{\text{avg}} = \frac{T_B - T_{\text{trn}}}{T_B} R_{\text{trn}}, \quad (39)$$

where  $T_{\text{trn}}$  is the beam training duration and  $R_{\text{trn}}$  is the average rate after the alignment. For the proposed method,  $R_{\text{trn}}$  is determined from rate plots when using the different array sizes (Fig. 7(a) shows a rate plot when using  $16 \times 16$  arrays). We assume optimistically that IEEE 802.11ad achieves the perfect alignment rate. While the average rate of the proposed beam alignment keeps increasing as the array size increases, that of IEEE 802.11ad increases slowly at 10 m/s or starts to decrease at speed beyond 15 m/s when the array becomes larger than  $16 \times 16$ . We also observe that when the average rate of IEEE 802.11ad becomes zero when  $N_a$  at around 800 and 1000 when the speed is 15 and 20 m/s, respectively. This is because the training duration becomes larger than  $T_B$  so that there is no time left for data communication.



(a) Beam training duration versus the number of antenna elements.



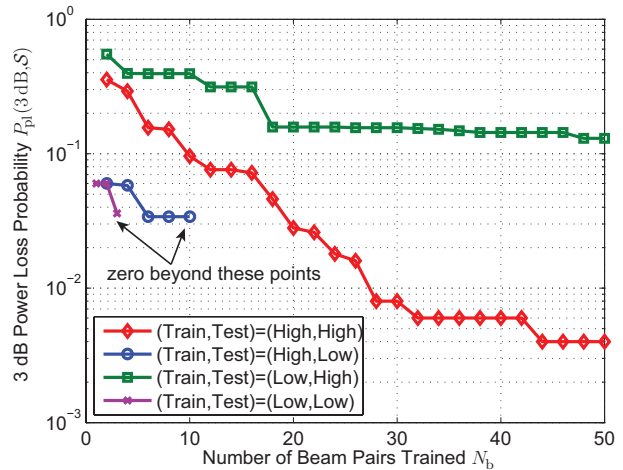
(b) Average rate considering beam training overhead (transmit power of 0 dBm).

Fig. 10. Overhead comparison between the proposed method and that of IEEE 802.11ad.

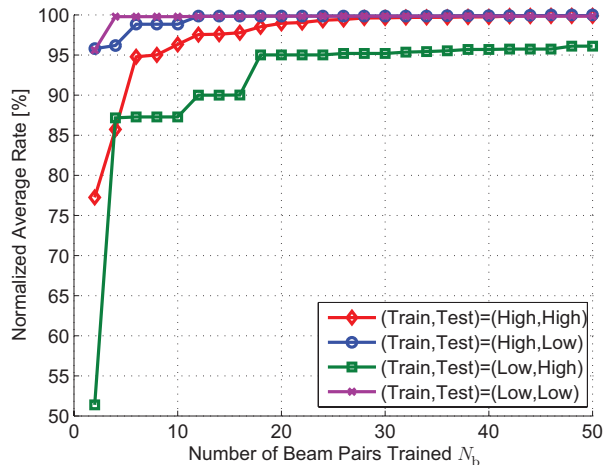
### E. Sensitivity to Change in Traffic Density

In this final subsection, we provide some simulation results to show the effect of the change in vehicular traffic density. To do this, we generated another dataset of 500 channel samples using the ray-tracing simulation with the same setting as described in Section II-A but with a lower vehicular traffic using  $\mu_\zeta = 0.0536$  (average vehicle gap of 18.66 m) and the car-to-truck ratio of 9:1. We use all combinations of these two datasets as the training and test set to evaluate the performance of the proposed beam alignment, namely the four combinations of training and test set of (low,low), (high,low), (low,high), and (high,high). We note that (high,high) is what is used so far. AvgPow is used as the selection method here.

Fig. 11 shows the performance in terms of the 3 dB power loss probability and the average rate normalized by the perfect beam alignment case when using EIRP of 24 dBm. When testing with the low traffic dataset, training (i.e., building the fingerprint database) using either the low or high traffic dataset yields good performance. Training using the low traffic dataset



(a) 3 dB power loss probability.



(b) Normalized averaged rate when EIRP=24 dBm.

Fig. 11. Sensitivity to change in traffic conditions.

(i.e., matched traffic condition) is slightly more efficient. On the contrary, when testing with the high traffic dataset, training using the low traffic dataset results in much worse performance than when training using the high traffic dataset. Intuitively, this is because the low traffic dataset cannot adequately capture paths in the richer scattering environment of the high traffic condition. The same trend can be confirmed in the rate plot in Fig. 11(b). These results show that building the database in the same traffic condition as when the database is used provides the best performance. If adaptation to traffic condition is not possible or costly, then training should be conducted in high traffic conditions.

## VII. CONCLUSION

We proposed an efficient beam alignment method for mmWave V2I communications leveraging position information and multipath fingerprints. Three types of fingerprints and two beam selection methods were proposed. The results show that when Type A fingerprints are available, which can capture correlation between beam pairs, minimizing the misalignment

probability is the best method for beam selection. If Type A is not possible, then our proposed heuristic beam selection using the average power should be used. Regarding the overhead of the beam training, our approach requires training about 30 beam pairs when  $16 \times 16$  arrays are used and the overhead increases roughly linearly with the number of antenna elements. The overhead calculation under the mobility context using the beam coherence time shows that while the proposed approach consumes less than a few percent of the beam coherence time for training, the IEEE 802.11ad beam training duration can exceed the beam coherence time for large arrays such as  $32 \times 32$ . It is also shown that when adaptation to traffic conditions is not possible, fingerprints should be collected during dense traffic conditions so that most possible paths can be captured in the database. This work demonstrates that side information can be exploited to improve the efficiency of mmWave communications, which is not only desirable but also necessary in vehicular settings.

#### REFERENCES

- [1] J. Levinson *et al.*, "Towards fully autonomous driving: Systems and algorithms," in *Proc. of the 2011 IEEE Intelligent Vehicles Symposium*, Jun. 2011, pp. 163–168.
- [2] J. B. Kenney, "Dedicated short-range communications (DSRC) standards in the United States," *Proceedings of the IEEE*, vol. 99, no. 7, pp. 1162–1182, Jul. 2011.
- [3] G. Araniti, C. Campolo, M. Condoluci, A. Iera, and A. Molinaro, "LTE for vehicular networking: A survey," *IEEE Communications Magazine*, vol. 51, no. 5, pp. 148–157, May 2013.
- [4] J. Choi, V. Va, N. Gonzalez-Prelcic, R. C. Daniels, C. R. Bhat, and R. W. Heath Jr., "Millimeter-wave vehicular communication to support massive automotive sensing," *IEEE Communications Magazine*, vol. 54, no. 12, pp. 160–167, Dec. 2016.
- [5] V. Va, T. Shimizu, G. Bansal, and R. W. Heath Jr., "Millimeter wave vehicular communications: A survey," *Foundations and Trends in Networking*, vol. 10, no. 1, pp. 1–113, 2016.
- [6] P. Bahl and V. N. Padmanabhan, "RADAR: an in-building RF-based user location and tracking system," in *Proc. of the IEEE INFOCOM*, Mar. 2000, pp. 775–784.
- [7] B. D. S. Lakmali and D. Dias, "Database correlation for GSM location in outdoor & indoor environments," in *Proc. of the 4th International Conference on Information and Automation for Sustainability*, Dec. 2008, pp. 42–47.
- [8] E. Kupershtein, M. Wax, and I. Cohen, "Single-site emitter localization via multipath fingerprinting," *IEEE Trans. Signal Process.*, vol. 61, no. 1, pp. 10–21, 2013.
- [9] E. Ward and J. Folkesson, "Vehicle localization with low cost radar sensors," in *Proc. IEEE Intelligent Vehicles Symposium*, Jun. 2016, pp. 864–870.
- [10] T. S. Rappaport, F. Gutierrez, E. Ben-Dor, J. N. Murdock, Y. Qiao, and J. I. Tamir, "Broadband millimeter-wave propagation measurements and models using adaptive-beam antennas for outdoor urban cellular communications," *IEEE Transactions on Antennas and Propagation*, vol. 61, no. 4, pp. 1850–1859, Apr. 2013.
- [11] V. Va, J. Choi, and R. W. Heath Jr., "The impact of beamwidth on temporal channel variation in vehicular channels and its implications," *IEEE Transactions on Vehicular Technology*, vol. PP, no. 99, pp. 1–1, 2016.
- [12] Remcom, "Wireless InSite," <http://www.remcom.com/wireless-insite>.
- [13] J. Wang, Z. Lan, C. woo Pyo, T. Baykas, C.-S. Sum, M. Rahman, J. Gao, R. Funada, F. Kojima, H. Harada, and S. Kato, "Beam codebook based beamforming protocol for multi-Gbps millimeter-wave WPAN systems," *IEEE J. on Sel. Areas in Commun.*, vol. 27, no. 8, pp. 1390–1399, Oct. 2009.
- [14] S. Hur, T. Kim, D. J. Love, J. V. Krogmeier, T. A. Thomas, and A. Ghosh, "Millimeter wave beamforming for wireless backhaul and access in small cell networks," *IEEE Trans. Commun.*, vol. 61, no. 10, pp. 4391–4403, Oct. 2013.
- [15] K. Hosoya, N. Prasad, K. Ramachandran, N. Orihashi, S. Kishimoto, S. Rangarajan, and K. Maruhashi, "Multiple sector ID capture (MIDC): A novel beamforming technique for 60-GHz band multi-Gbps WLAN/PAN systems," *IEEE Trans. Antennas Propag.*, vol. 63, no. 1, pp. 81–96, Jan. 2015.
- [16] T. Kim and D. J. Love, "Virtual AoA and AoD estimation for sparse millimeter wave MIMO channels," in *Proc. of the IEEE Workshop on Signal Processing Advances in Wireless Communications*, 2015, pp. 146–150.
- [17] Q. Duan, T. Kim, H. Huang, K. Liu, and G. Wang, "AoD and AoA tracking with directional sounding beam design for millimeter wave MIMO systems," in *Proc. of the IEEE International Symposium on Personal, Indoor and Mobile Radio Communications*, Aug. 2015, pp. 2271–2276.
- [18] Z. Marzi, D. Ramasamy, and U. Madhoo, "Compressive channel estimation and tracking for large arrays in mm-wave picocells," *IEEE Journal of Selected Topics in Signal Processing*, vol. 10, no. 3, pp. 514–527, 2016.
- [19] B. Li, Z. Zhou, W. Zou, X. Sun, and G. Du, "On the efficient beamforming training for 60 GHz wireless personal area networks," *IEEE Transactions on Wireless Communications*, vol. 12, no. 2, pp. 504–515, 2013.
- [20] B. Li, Z. Zhou, H. Zhang, and A. Nallanathan, "Efficient beamforming training for 60-GHz millimeter-wave communications: A novel numerical optimization framework," *IEEE Transactions on Vehicular Technology*, vol. 63, no. 2, pp. 703–717, 2014.
- [21] T. Kadur, H.-I. Chiang, and G. Fettweis, "Effective beam alignment algorithm for low cost millimeter wave communication," in *Proc. of the IEEE Vehicular Technology Conference*, 2016, pp. 1–5.
- [22] J. Kim and A. F. Molisch, "Enabling Gigabit services for IEEE 802.11ad-capable high-speed train networks," in *Proc. of the IEEE RWS*, Jan. 2013, pp. 145–147.
- [23] V. Va, T. Shimizu, G. Bansal, and R. W. Heath Jr., "Beam design for beam switching based millimeter wave vehicle-to-infrastructure communications," in *Proc. of the IEEE International Conference on Communications*, May 2016, pp. 1–6.
- [24] N. Gonzalez-Prelcic, R. Mendez-Rial, and R. W. Heath Jr., "Radar aided beam alignment in mmwave V2I communications supporting antenna diversity," in *Proceedings of the 2016 Information Theory and Applications Workshop*, Feb. 2016.
- [25] T. Nitsche, A. B. Flores, E. W. Knightly, and J. Widmer, "Steering with eyes closed: Mm-wave beam steering without in-band measurement," in *Proc. IEEE INFOCOM*, vol. 26, 2015, pp. 2416–2424.
- [26] A. Ali and R. W. Heath Jr., "Compressed beam selection in millimeter wave systems with out-of-band partial support information," in *Proc. of the IEEE International Conf. on Acoustics, Speech and Signal Processing*, 2017.
- [27] "IEEE std 802.15.3c-2009," *IEEE Standard*, pp. c1–187, Oct. 2009.
- [28] "IEEE std 802.11ad-2012," *IEEE Standard*, pp. 1–628, Dec. 2012.
- [29] A. S. Al-Ghamdi, "Analysis of time headways on urban roads: Case study from riyadh," *Transport Eng-J*, vol. 127, no. 4, pp. 289–294, 2001.
- [30] K. Mase, J. Inoue, and J. Kizu, "Performance evaluation of a roadside-to-vehicle communication system using narrow antenna beam switching based on traffic flow model," in *Proc. of the IEEE Globecom Workshops*, 2008, pp. 1–5.
- [31] R. W. Heath Jr., *Introduction to Wireless Digital Communication: A Signal Processing Perspective*. Prentice Hal, Mar. 2017.
- [32] G. Grimmett and D. Stirzaker, *Probability and Random Processes*, 3rd ed. Oxford University Press, 2001.
- [33] J. Edmonds, "Matroids and the greedy algorithm," *Mathematical Programming*, vol. 1, no. 1, pp. 127–136, 1971.
- [34] G. Calinescu, C. Chekuri, M. Pál, and J. Vondrák, "Maximizing a monotone submodular function subject to a matroid constraint," *SIAM J. Comput.*, vol. 40, no. 6, pp. 1740–1766, Dec. 2011.
- [35] G. L. Nemhauser, L. A. Wolsey, and M. L. Fisher, "An analysis of approximations for maximizing submodular set functions-I," *Mathematical Programming*, vol. 14, no. 1, pp. 265–294, 1978.
- [36] T. J. Hastie, R. J. Tibshirani, and J. H. Friedman, *The Elements of Statistical Learning : Data Mining, Inference, and Prediction*, ser. Springer series in statistics. New York: Springer, 2009.
- [37] S. J. Orfanidis, *Electromagnetic Waves and Antenna*. Rutgers University, 2014, online book <http://www.ece.rutgers.edu/~orfanidi/ewal/>.